Original Article

Journal of LOW FREQUENCY NOISE, VIBRATION AND ACTIVE CONTROL

Journal of Low Frequency Noise, Vibration and Active Control
2019, Vol. 38(2) 558–573

DOI: 10.1177/1461348418817465
journals.sagepub.com/home/lfn
SAGE

Thermoelastic coupling vibration and stability analysis of rotating circular plate in friction clutch

Yongqiang Yang[1,2], Zhongmin Wang[3] and Yongqin Wang[1,2]

Abstract

Rotating friction circular plates are the main components of a friction clutch. The vibration and temperature field of these friction circular plates in high speed affect the clutch operation. This study investigates the thermoelastic coupling vibration and stability of rotating friction circular plates. Firstly, based on the middle internal forces resulting from the action of normal inertial force, the differential equation of transverse vibration with variable coefficients for an axisymmetric rotating circular plate is established by thin plate theory and thermal conduction equation considering deformation effect. Secondly, the differential equation of vibration and corresponding boundary conditions are discretized by the differential quadrature method. Meanwhile, the thermoelastic coupling transverse vibrations with three different boundary conditions are calculated. In this case, the change curve of the first two-order dimensionless complex frequencies of the rotating circular plate with the dimensionless angular speed and thermoelastic coupling coefficient are analyzed. The effects of the critical dimensionless thermoelastic coupling coefficient and the critical angular speed on the stability of the rotating circular plate with simply supported and clamped edges are discussed. Finally, the relation between the critical divergence speed and the dimensionless thermoelastic coupling coefficient is obtained. The results provide the theoretical basis for optimizing the structure and improving the dynamic stability of friction clutches.

Keywords

Rotating circular plate, friction clutch, transverse vibration, thermoelastic coupling, differential quadrature method, stability

Introduction

Friction clutch is an important part of the transmission system of mineral locomotives. Considering the mining industry background, the friction clutch of Shaanxi XUST-18 explosion-proof mineral locomotive (shown in Figure 1) is used as the sample. By considering friction circular plate as the thin plate (shown in Figure 2), the clutch active shells can be regarded as the boundary supports. Friction circular plates in clutch often work in a varying temperature field; thus, the transverse vibration originated from the varying temperature generally has a significant influence on the operation of the mineral locomotive. Therefore, a study on the thermoelastic coupling transverse vibration of the friction circular plates in clutch is important.

Transverse vibration of the rotating circular plate has been extensively studied over the past few decades, and numerous representative results have been achieved. Some research work focus on the effects of angular speed on transverse vibration. For example, Khorasany and Hutton[1] and Shojaeefard et al.[2] investigated the variation of

[1]School of Mechanical and Precision Instrument Engineering, Xi'an University of Technology, Xi'an, China
[2]College of Mechanical & Electrical Engineering, Shaanxi University of Science & Technology, Xi'an, China
[3]School of Civil Engineering and Architecture, Xi'an University of Technology, Xi'an, China

Corresponding author:
Zhongmin Wang, School of Civil Engineering and Architecture, Xi'an University of Technology, No. 5 South Jinhua Road, 710048 Xi'an, China.
Email: wangzhongm@xaut.edu.cn

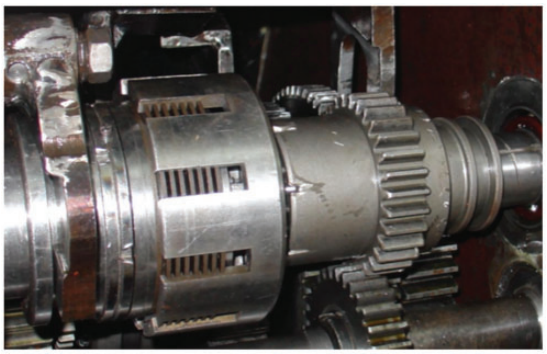

Figure 1. Friction clutch in Shaanxi XUST-18 explosion-proof mineral locomotive.

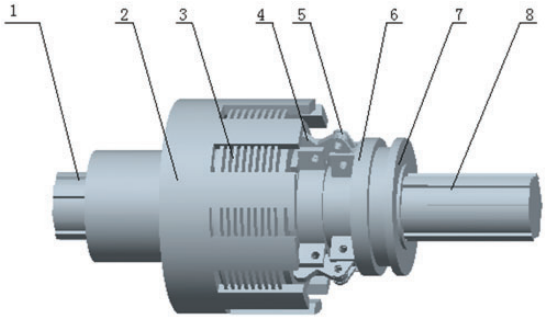

Figure 2. Three-dimensional model of friction clutch: 1, driving shaft; 2, clutch active shell; 3, friction plate combination; 4, hinge mechanism; 5, pin; 6, clutch member; 7, clutch driven member; and 8, driven shaft.

the natural frequency with the angular speed of the rotating circular plate by the modal expansion method and the Galerkin method, respectively. Maretic[3] used the Galerkin method to analyze the relationship between the natural frequency of the eccentric rotating circular plate and angular speed. Wang et al.[4,5] analyzed the change situation of the complex frequencies of the rotating circular plate under three boundary conditions with the change of the angular speed. The aforementioned research works have not considered the transverse deflections and dynamic responses. Gupta et al.[6] utilized Rayleigh-Ritz method to calculate the deflections of the first two modes in orthotropic viscoelastic circular plates and discussed the effect of nonhomogeneous value and taper coefficient on the transverse vibration of the circular plate. Heo and Chung[7] studied the dynamic responses of a flexible rotating plate by finite element method and examined the relationship between the vibration characteristics and angular misalignment of the circular plate. On the other hand, some researchers focus on the dynamic stability of the circular plate. Bauer and Eidel[8] analyzed the effects of angular speed on natural frequency and stability by the Galerkin method. Hochlenert et al.[9] studied the instability problem of the circular plate caused by the friction in the brake system. Mottershead and Chan[10] examined the flutter instability of the circular plate under the frictional follower load. Hu and Wang[11] and Li et al.[12] established the magnetoelastic vibration equations of a conductive rotating circular plate by Hamilton principle. They investigated the critical condition of stability of the rotating circular plate by the Galerkin method.

All of the aforementioned studies do not involve the varying temperature. In fact, the circular plate is under the condition of varying temperature environment in actual engineering applications (e.g. the engaging process of friction clutch), so the varying temperature needs to be considered. Sepahi et al.[13] analyzed the effect of varying temperature on the large deflection of the FGM plate. Shu and Zhang[14] used the Galerkin method to discuss the nonlinear thermoelastic vibration of the circular plate with clamped edge. Trajkovski and Cukic[15] studied the vibration problem of the circular plate under the boundary of free and clamped edges with varying temperature. Sun and coworkers[16,17] analyzed the thermoelastic coupling vibration of micro-circular plates and discussed the effect of component size and different temperatures on the thermal bending moments and vibration amplitude. Salajeghe et al.[18] examined the thermoelastic vibration of micro-circular resonators by von Karman theory and explored the effect of linear and nonlinear analysis on thermoelastic damping. Hao[19] investigated the vibration of

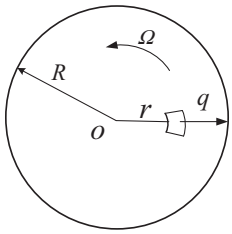

Figure 3. Schematic diagram for the rotating circular plate.

circular thin plate micrometer and nanometer electromechanical exciters under heat-elastic damping. Kumar et al.[20] studied a two-dimensional axisymmetric vibration in a homogeneous isotropic micropolar porous thermoelastic circular plate by using the eigenvalue approach and analyzed the displacements, microrotations, volume fraction fields, temperature distributions and stresses in the transformed domain subjected to thermo-mechanical sources. Bhada et al.[21] used integral transform technique to investigate the thermally induced vibration of an elliptical disk and discussed the thermal moment, normal stresses and normal deflection of disk. The above research works on the thermoelastic coupling vibration of circular plates are mainly focused on the analysis of the coupled term and dynamic term, but the research on the differential equation of thermoelastic coupling vibration is not that much. The differential equation of thermoelastic coupling vibration of the circular plate is a fourth-order partial differential equation with complex variable coefficient, which involves solving a complex eigenvalue problem. Some research work on a high-order partial differential equation had been carried out by the Galerkin method and finite element method.[1,3,7,8,11,12,22] Yayli[23–27] used the Fourier sine series and Stoke transformation to analyze the high-order partial differential equation of vibration. The computation in these methods is complicated. In recent years, the differential quadrature method (DQM) has also been applied to compute the high-order partial differential equation of transverse vibration because of its high efficiency and accuracy.[28–32] However, few works have been presented the study of the high-order partial differential equation of thermoelastic coupling vibration by DQM. In this paper, we mainly use the DQM to solve the differential equation of thermoelastic coupling vibration in order to improve the solving efficiency and accuracy.

This study aims to construct the differential equation of thermoelastic coupling transverse vibration of the rotating circular plate in friction clutch in accordance with the thermal conduction equation and on the basis of the action of linearly distributed normal inertial force along the radial direction. The dimensionless complex frequencies of the rotating circular plate with variable temperature are analyzed by DQM. The change curve of the first two-order dimensionless complex frequencies of the rotating circular plate with the dimensionless angular speed and the dimensionless thermoelastic coupling coefficient are analyzed, which can provide the theoretical basis for optimizing the structure and working condition of friction clutch.

Differential equation of thermoelastic coupling transverse vibration

Differential equation of transverse vibration with varying temperature

Figure 3 shows a circular plate with thickness h and radius R. The plate is rotating around its axis with a constant angular speed Ω. Meanwhile, ρ denotes the density of materials, r is the radius of the polar coordinate and $q = \rho h \Omega^2 r$ indicates the inertial force per unit area in the middle plane.

The strain–displacement relation of the rotating circular plate can be given by

$$\begin{cases} \varepsilon_r = \dfrac{\partial u_r}{\partial r} = -z\dfrac{\partial^2 w}{\partial r^2} \\ \varepsilon_\theta = \dfrac{u_r}{r} = -\dfrac{z}{r}\dfrac{\partial w}{\partial r} \end{cases} \tag{1}$$

where u_r is the displacement field component along the r axis, z represents the rotation axis and $w = w(r, t)$ refers to the transverse displacement.

The constitutive equation with the varying temperature T can be written as

$$\begin{cases} \sigma_r = \dfrac{E}{1-\mu^2}\left[(\varepsilon_r + \mu\varepsilon_\theta) - (1+\mu)\alpha T\right] \\ \sigma_\theta = \dfrac{E}{1-\mu^2}\left[(\varepsilon_\theta + \mu\varepsilon_r) - (1+\mu)\alpha T\right] \end{cases} \tag{2}$$

where E is the elastic modulus, μ is Poisson's ratio, and α denotes the linear thermal expansion coefficient.

Substituting equation (1) into equation (2) results in

$$\begin{cases} \sigma_r = \dfrac{-zE}{1-\mu^2}\left(\dfrac{\partial^2 w}{\partial r^2} + \dfrac{\mu}{r}\dfrac{\partial w}{\partial r}\right) - \dfrac{E\alpha T}{1-\mu} \\ \sigma_\theta = \dfrac{-zE}{1-\mu^2}\left(\dfrac{1}{r}\dfrac{\partial w}{\partial r} + \mu\dfrac{\partial^2 w}{\partial r^2}\right) - \dfrac{E\alpha T}{1-\mu} \\ \tau_{r\theta} = 0 \end{cases} \tag{3}$$

By using equation (3), the bending and twisting moments per unit length are given by

$$\begin{cases} M_r = \displaystyle\int_{-\frac{h}{2}}^{\frac{h}{2}} \sigma_r z \mathrm{d}z = -\mathrm{D}\left(\dfrac{\partial^2 w}{\partial r^2} + \dfrac{\mu}{r}\dfrac{\partial w}{\partial r}\right) - \dfrac{E\alpha}{1-\mu} M_T \\ M_\theta = \displaystyle\int_{-\frac{h}{2}}^{\frac{h}{2}} \sigma_\theta z \mathrm{d}z = -\mathrm{D}\left(\dfrac{1}{r}\dfrac{\partial w}{\partial r} + \mu\dfrac{\partial^2 w}{\partial r^2}\right) - \dfrac{E\alpha}{1-\mu} M_T \\ M_{r\theta} = 0 \end{cases} \tag{4}$$

where $D = \frac{Eh^3}{12(1-\mu^2)}$ is the flexural rigidity and $M_T = \displaystyle\int_{-\frac{h}{2}}^{\frac{h}{2}} Tz\mathrm{d}z$ indicates the thermal moment.

The force and moment balance condition in the axisymmetric circular plate are given by

$$\begin{cases} \dfrac{\partial N_r}{\partial r} + \dfrac{N_r - N_\theta}{r} + q = 0 \\ \dfrac{\partial M_r}{\partial r} + \dfrac{M_r - M_\theta}{r} - Q_r = 0 \\ \left(\dfrac{1}{r}Q_r + \dfrac{\partial Q_r}{\partial r}\right) + \left(N_r\dfrac{\partial^2 w}{\partial r^2} + \dfrac{1}{r}N_r\dfrac{\partial w}{\partial r} + \dfrac{\partial N_r}{\partial r}\dfrac{\partial w}{\partial r}\right) - \rho h\dfrac{\partial^2 w}{\partial t^2} + p = 0 \end{cases} \tag{5}$$

where N_R and N_θ represent the normal in-plane forces, p is the lateral load per unit area and Q_r refers to the lateral shear.

Based on equations (1)–(5), by using the Kirchhoff theory and D'Alembert's principle, the differential equation of transverse vibration is given as follows

$$D\nabla^4 w + \frac{E\alpha}{1-\mu}\nabla^2 M_T + \rho h\frac{\partial^2 w}{\partial t^2} - N_r\frac{\partial^2 w}{\partial r^2} - \frac{1}{r}N_\theta\frac{\partial w}{\partial r} + q\frac{\partial w}{\partial r} - p = 0 \tag{6}$$

Given that the varying temperature T along the lateral direction is considerably larger than that along radial direction, the thermal conduction equation can be described as follows

$$\frac{\partial T}{\partial t} - \frac{k}{\rho C_v}\frac{\partial^2 T}{\partial z^2} + \frac{E\alpha T_0}{(1-2\mu)\rho C_v}\frac{\partial}{\partial t}\left(-z\frac{\partial^2 w}{\partial r^2} - z\frac{1}{r}\frac{\partial w}{\partial r}\right) = 0 \tag{7}$$

where $T = T(z,t)$ is the varying temperature, k denotes the thermal conductivity, C_v indicates the specific heat at a constant volume and T_0 represents the initial temperature of the circular plate.

M_T in the differential equation (6) is related to $T(z,t)$, and the thermal conduction equation (7) involves the deflection function $w = w(r,t)$. It can be seen that the temperature and deflection fields are coupled together. In this way, equations (6) and (7) must be solved simultaneously.

Solution of the normal in-plane forces

In order to solve equations (6) and (7), the normal in-plane forces N_r and N_θ need to be solved firstly. The stress function φ is introduced

$$\begin{cases} \varphi = r\sigma_r \\ \sigma_\theta = \dfrac{\mathrm{d}\varphi}{\mathrm{d}r} + \rho\Omega^2 r^2 \end{cases} \tag{8}$$

Based on equation (1), the strain compatibility equation is obtained

$$\varepsilon_r = \frac{\partial(r\varepsilon_\theta)}{\partial r} \tag{9}$$

Considering that the varying temperature T along the radial direction is ignored, the compatibility equation is obtained

$$r^2\frac{\mathrm{d}^2\varphi}{\mathrm{d}r^2} + r\frac{\mathrm{d}\varphi}{\mathrm{d}r} - \varphi = -(3+\mu)\rho\Omega^2 r^3 \tag{10}$$

From equation (10), the solution of $\varphi(r)$ can be obtained as

$$\varphi(r) = Ar + \frac{B}{r} - \frac{3+\mu}{8}\rho\Omega^2 r^3 \tag{11}$$

where A and B are integral constants. Integral constant B must be zero since the stress at the center of the circular plate ($r = 0$) is a finite value.

The displacement field component u_r along the radial direction of the plate is as follows

$$u_r = \frac{r}{E}\left[(1-\mu)A - (1-\mu)\frac{B}{r^2} + \frac{\mu^2-1}{8}\rho\Omega^2 r^2\right] \tag{12}$$

The boundary conditions of clamped and simply supported edges are given by

$$u_r|_{r=R} = 0 \tag{13}$$

The boundary condition of free edge is given by

$$\sigma_r|_{r=R} = 0 \tag{14}$$

Substituting equations (11) and (12) into equations (13) and (14), respectively, results in

$$A = \begin{cases} \dfrac{1+\mu}{8}\rho\Omega^2 R^2 \text{ clamped and simply supported edges} \\ \dfrac{3+\mu}{8}\rho\Omega^2 R^2 \text{ free edge} \end{cases} \tag{15}$$

For clamped and simply supported edges, based on equations (8), (11) and (15), N_r and N_θ can be obtained as

$$N_r = h\sigma_r = \rho\Omega^2 h\left(\frac{1+\mu}{8}R^2 - \frac{3+\mu}{8}r^2\right) \tag{16}$$

$$N_\theta = h\sigma_\theta = \rho\Omega^2 h\left(\frac{1+\mu}{8}R^2 - \frac{1+3\mu}{8}r^2\right) \tag{17}$$

For free edge, based on equations (8), (11) and (15), N_R and N_θ are given by

$$N_r = h\sigma_r = \frac{\rho\Omega^2 R^2 h(3+\mu)}{8}\left(1 - \frac{r^2}{R^2}\right) \tag{18}$$

$$N_\theta = h\sigma_\theta = \frac{\rho\Omega^2 R^2 h}{8}\left((3+\mu) - (1+3\mu)\frac{r^2}{R^2}\right) \tag{19}$$

Dimensionless differential equation and boundary conditions

The following dimensionless quantities are introduced as follows

$$\bar{r} = \frac{r}{R}, \quad \bar{z} = \frac{z}{h}, \quad \bar{w} = \frac{w}{h}, \quad \bar{T} = \frac{T}{T_0}, \quad \tau = \frac{th}{R^2}\sqrt{\frac{E}{12\rho(1-\mu^2)}}, \quad c = \frac{\rho R^4\Omega^2}{Eh^2}$$

Considering that $p = 0$, equations (6) and (7) take the form of

$$\left(\frac{\partial^4\bar{w}}{\partial\bar{r}^4} + \frac{2}{\bar{r}}\frac{\partial^3\bar{w}}{\partial\bar{r}^3} - \frac{1}{\bar{r}^2}\frac{\partial^2\bar{w}}{\partial\bar{r}^2} + \frac{1}{\bar{r}^3}\frac{\partial\bar{w}}{\partial\bar{r}}\right) + A_1\left(\frac{\partial^2\bar{M}_T}{\partial\bar{r}^2} + \frac{1}{\bar{r}}\frac{\partial\bar{M}_T}{\partial\bar{r}}\right) + \frac{\partial^2\bar{w}}{\partial\tau^2} - \eta\left(N_1\frac{\partial^2\bar{w}}{\partial\bar{r}^2} + N_2\frac{1}{\bar{r}}\frac{\partial\bar{w}}{\partial\bar{r}} - c\bar{r}\frac{\partial\bar{w}}{\partial\bar{r}}\right) = 0 \tag{20}$$

$$\frac{\partial^2\bar{T}}{\partial\bar{z}^2} - A_2\frac{\partial\bar{T}}{\partial\tau} + A_3\frac{\partial}{\partial\tau}\left(\frac{\partial^2\bar{w}}{\partial\bar{r}^2} + \frac{1}{\bar{r}}\frac{\partial\bar{w}}{\partial\bar{r}}\right)\bar{z} = 0 \tag{21}$$

where $\bar{M}_T = \int_{-1/2}^{1/2}\bar{T}\bar{z}\mathrm{d}\bar{z}$, $\eta = 12(1-\mu^2)$, $A_1 = \frac{12(1+\mu)R^2\alpha T_0}{h^2}$, $A_2 = \frac{C_v h^3}{kR^2}\sqrt{\frac{\rho E}{12(1-\mu^2)}}$, $A_3 = \frac{E\alpha h^5}{(1-2\mu)kR^4}\sqrt{\frac{E}{12\rho(1-\mu^2)}}$

For simply supported and clamped edges, N_1 and N_2 are as follows

$$N_1 = \frac{c}{8}\left[(1+\mu) - (3+\mu)\bar{r}^2\right] \tag{22}$$

$$N_2 = \frac{c}{8}\left[(1+\mu) - (1+3\mu)\bar{r}^2\right] \tag{23}$$

For free edge, N_1 and N_2 are as follows

$$N_1 = \frac{c}{8}\left[(3+\mu) - (3+\mu)\bar{r}^2\right] \tag{24}$$

$$N_2 = \frac{c}{8}\left[(3+\mu) - (1+3\mu)\bar{r}^2\right] \tag{25}$$

The solution of equations (20) and (21) is assumed in the following form

$$\bar{w}(\bar{r},\tau) = W(\bar{r})e^{\mathrm{j}\omega\tau} \quad \bar{T}(\bar{z},\tau) = T^*(\bar{z})e^{\mathrm{j}\omega\tau} \tag{26}$$

where $\mathrm{j} = \sqrt{-1}$, ω denotes the dimensionless complex frequency of the rotating circular plate.

Substituting equation (26) into equations (20) and (21), differential equations of the rotating plate are obtained as

$$\left(\frac{\mathrm{d}^4W}{\mathrm{d}\bar{r}^4}+\frac{2}{\bar{r}}\frac{\mathrm{d}^3W}{\mathrm{d}\bar{r}^3}-\frac{1}{\bar{r}^2}\frac{\mathrm{d}^2W}{\mathrm{d}\bar{r}^2}+\frac{1}{\bar{r}^3}\frac{\mathrm{d}W}{\mathrm{d}\bar{r}}\right)+A_1\left(\frac{\mathrm{d}^2}{\mathrm{d}\bar{r}^2}+\frac{1}{\bar{r}}\frac{\mathrm{d}}{\mathrm{d}\bar{r}}\right)\int_{-1/2}^{1/2}T^*\bar{z}\mathrm{d}\bar{z}$$
$$-\omega^2W-\eta\left(N_1\frac{\mathrm{d}^2W}{\mathrm{d}\bar{r}^2}+N_2\frac{1}{\bar{r}}\frac{\mathrm{d}W}{\mathrm{d}\bar{r}}-c\bar{r}\frac{\mathrm{d}W}{\mathrm{d}\bar{r}}\right)=0 \tag{27}$$

$$\frac{\mathrm{d}^2T^*}{\mathrm{d}\bar{z}^2}-A_2\mathrm{j}\omega T^*+A_3\mathrm{j}\omega\left(\frac{\mathrm{d}^2W}{\mathrm{d}\bar{r}^2}+\frac{1}{\bar{r}}\frac{\mathrm{d}W}{\mathrm{d}\bar{r}}\right)\bar{Z}=0 \tag{28}$$

From equation (28), the solution of T^* can be obtained as

$$T^*=a_1e^{b\bar{z}}+a_2e^{-b\bar{z}}+\frac{E\alpha h^2}{(1-2\mu)\rho C_vR^2}\left(\frac{\mathrm{d}^2W}{\mathrm{d}\bar{r}^2}+\frac{1}{\bar{r}}\frac{\mathrm{d}W}{\mathrm{d}\bar{r}}\right)\bar{z} \tag{29}$$

where a_1 and a_2 are two integral constants and $b=\sqrt{A_2\mathrm{j}\omega}$.

Substituting equation (29) into equation (27) results in

$$(1+\psi)\left(\frac{\mathrm{d}^4W}{\mathrm{d}\bar{r}^4}+\frac{2}{\bar{r}}\frac{\mathrm{d}^3W}{\mathrm{d}\bar{r}^3}-\frac{1}{\bar{r}^2}\frac{\mathrm{d}^2W}{\mathrm{d}\bar{r}^2}+\frac{1}{\bar{r}^3}\frac{\mathrm{d}W}{\mathrm{d}\bar{r}}\right)-\omega^2W-\eta\left(N_1\frac{\mathrm{d}^2W}{\mathrm{d}\bar{r}^2}+N_2\frac{1}{\bar{r}}\frac{\mathrm{d}W}{\mathrm{d}\bar{r}}-c\bar{r}\frac{\mathrm{d}W}{\mathrm{d}\bar{r}}\right)=0 \tag{30}$$

where $\psi=\frac{(1+\mu)E\alpha^2T_0}{(1-2\mu)\rho C_v}$ is the dimensionless thermoelastic coupling coefficient and indicates the coupling degree between the temperature and strain.

The dimensionless thermoelastic coupling coefficient ψ is composed of five parameters, which are the elastic modulus E, Poisson's ratio μ, the linear thermal expansion coefficient α, the density of material ρ and the initial temperature T_0 of the circular plate. The dimensionless thermoelastic coupling coefficient is related to the initial temperature for a given material. With the increase of initial temperature, the dimensionless thermoelastic coupling coefficient increases. Generally, the dimensionless thermoelastic coupling coefficient ψ of most materials is between 0 and 0.5, but ψ of new materials may be higher.[33] When the plate material in the friction clutch is selected as No. 45 steel, the initial temperature of the friction plate is related to the number of engagement during the working process. With greater number of engagement, the initial temperature will be higher and the dimensionless thermoelastic coupling coefficient is larger. Based on the material and number of engagement of the friction plate, the study range of ψ in this paper is assumed to be 0–1.

Considering that the edge of the plate is held at a constant temperature, the three dimensionless boundary conditions are given as follows.

(1) Simply supported edge

$$\begin{cases} W|_{\bar{r}=1}=0 \\ \left(\dfrac{\mathrm{d}^2W}{\mathrm{d}\bar{r}^2}+\mu\dfrac{1}{\bar{r}}\dfrac{\mathrm{d}W}{\mathrm{d}\bar{r}}\right)|_{\bar{r}=1}=0 \end{cases} \tag{31}$$

(2) Clamped edge

$$\begin{cases} W|_{\bar{r}=1}=0 \\ \dfrac{\mathrm{d}W}{\mathrm{d}\bar{r}}|_{\bar{r}=1}=0 \end{cases} \tag{32}$$

(3) Free edge

$$\begin{cases} \left(\dfrac{\mathrm{d}^2W}{\mathrm{d}\bar{r}^2}+\mu\dfrac{1}{\bar{r}}\dfrac{\mathrm{d}W}{\mathrm{d}\bar{r}}\right)|_{\bar{r}=1}=0 \\ \left(\dfrac{\mathrm{d}^3W}{\mathrm{d}\bar{r}^3}+\dfrac{1}{\bar{r}}\dfrac{\mathrm{d}^2W}{\mathrm{d}\bar{r}^2}-\dfrac{1}{\bar{r}^2}\dfrac{\mathrm{d}W}{\mathrm{d}\bar{r}}\right)|_{\bar{r}=1}=0 \end{cases} \tag{33}$$

The dimensionless boundary conditions at the center of the plate are given as follows

$$\begin{cases} \dfrac{\mathrm{d}W}{\mathrm{d}\bar{r}}|_{\bar{r}=0} = 0 \\ \lim\limits_{\bar{r}\to 0}\left(\dfrac{\mathrm{d}^3 W}{\mathrm{d}\bar{r}^3} + \dfrac{1}{\bar{r}}\dfrac{\mathrm{d}^2 W}{\mathrm{d}\bar{r}^2} - \dfrac{1}{\bar{r}^2}\dfrac{\mathrm{d}W}{\mathrm{d}\bar{r}}\right) = 0 \end{cases} \tag{34}$$

Discretization method of vibration equation

DQM is used to solve equation (30). DQM[34–36] approximates the derivatives of the function at the given nodes by weighted sums of the function at the total nodes.

The nodes are calculated by the following formula

$$\bar{r}_1 = 0\,, \quad \bar{r}_N = 1, \quad \bar{r}_i = \frac{1}{2}\left(1 - \cos\frac{(2i-3)\pi}{2N-4}\right) \quad (i = 2, 3, \ldots, N-1) \tag{35}$$

Based on the Lagrange interpolation polynomial, the weight coefficients of the first derivative $A_{ij}^{(1)}$ are obtained

$$A_{ij}^{(1)} = \begin{cases} \prod\limits_{\substack{k=1 \\ k\neq i,j}}^{N}(x_i - x_k)/\prod\limits_{\substack{k=1 \\ k\neq j}}^{N}(x_j - x_k) & (i,j = 1,2,\ldots,N; i \neq j) \\ \sum\limits_{\substack{k=1 \\ k\neq j}}^{N}\dfrac{1}{(x_i - x_k)} & (i,\ j = 1,2,\ldots,N; i = j) \end{cases} \tag{36}$$

The weight coefficients of the second, third and fourth derivatives are determined by matrix multiplication

$$\begin{cases} A_{ij}^{(2)} = \sum\limits_{k=1}^{N} A_{ik}^{(1)} A_{kj}^{(1)} \\ A_{ij}^{(3)} = \sum\limits_{k=1}^{N} A_{ik}^{(2)} A_{kj}^{(1)} \quad (i,j = 1,2,\ldots,N) \\ A_{ij}^{(4)} = \sum\limits_{k=1}^{N} A_{ik}^{(3)} A_{kj}^{(1)} \end{cases} \tag{37}$$

Equation (30) can be discretized into the following form by DQM

$$\begin{aligned} &(1+\psi)\left(\sum_{k=1}^{N} A_{ik}^{(4)} W_k + \frac{2}{\bar{r}_i}\sum_{k=1}^{N} A_{ik}^{(3)} W_k - \frac{1}{\bar{r}_i{}^2}\sum_{k=1}^{N} A_{ik}^{(2)} W_k + \frac{1}{\bar{r}_i{}^3}\sum_{k=1}^{N} A_{ik}^{(1)} W_k\right) \\ &-\eta\left(N_{1i}\sum_{k=1}^{N} A_{ik}^{(2)} W_k + N_{2i}\frac{1}{\bar{r}_i}\sum_{k=1}^{N} A_{ik}^{(1)} W_k - c\bar{r}_i\sum_{k=1}^{N} A_{ik}^{(1)} W_k\right) - \omega^2 W_i = 0 \end{aligned} \tag{38}$$

The discretization of equations (31) to (33)can be can be expressed as follows.

(1) Simply supported edge

$$\begin{cases} W_N = 0 \\ \sum\limits_{k=1}^{N} A_{(N-1)k}^{(2)} W_k + \mu\dfrac{1}{\bar{r}_{(N-1)}}\sum\limits_{k=1}^{N} A_{(N-1)k}^{(1)} W_k = 0 \end{cases} \tag{39}$$

(2) Clamped edge

$$\begin{cases} W_N = 0 \\ \sum\limits_{k=1}^{N} A_{(N-1)k}^{(1)} W_k = 0 \end{cases} \tag{40}$$

(3) Free edge

$$\begin{cases} \sum_{k=1}^{N} A_{Nk}^{(2)} W_k + \mu \frac{1}{\bar{r}_N} \sum_{k=1}^{N} A_{Nk}^{(1)} W_k = 0 \\ \sum_{k=1}^{N} A_{(N-1)k}^{(3)} W_k + \frac{1}{\bar{r}_{(N-1)}} \sum_{k=1}^{N} A_{(N-1)k}^{(2)} W_k - \frac{1}{\bar{r}^2{}_{(N-1)}} \sum_{k=1}^{N} A_{(N-1)k}^{(1)} W_k = 0 \end{cases} \tag{41}$$

The discretization of equation (34) can be expressed in the following form

$$\begin{cases} \sum_{k=1}^{N} A_{1k}^{(1)} W_k = 0 \\ \sum_{k=1}^{N} A_{2k}^{(3)} W_k + \frac{1}{\bar{r}_2} \sum_{k=1}^{N} A_{2k}^{(2)} W_k - \frac{1}{\bar{r}_2^2} \sum_{k=1}^{N} A_{2k}^{(1)} W_k = 0 \end{cases} \tag{42}$$

Equation (38), the boundary condition (equation (42)), and one of the boundary conditions (equations (39)–(41)) can be expressed in the matrix form as

$$(\omega^2[I] + [K])\{W\} = 0 \tag{43}$$

where $[I]$ is identity matrix, the matrix $[K]$ involves the dimensionless angular speed c and the dimensionless thermoelastic coupling coefficient ψ.

Numerical analysis

Equation (38) is simplified to the differential equation of transverse vibration of the nonrotating plate at a constant temperature when $\psi = 0$ and $c = 0$. The first four-order natural frequencies of the nonrotating plate with three boundary conditions are calculated when the number of nodes $N = 9, 10, 11, 13, 15$. The calculation results are in good agreement with those exhibited by Ni,[37] which can be seen in Table 1. It shows when the number of nodes N is greater than 13, the value of the natural frequency has stabilized. In addition, Han and Liew[31] also mentioned when N is greater than 13, it can obtain the converged results by DQM. Therefore, $N = 13$ is selected in this study by considering the accuracy and stability of DQM.

Rotating circular plate in friction clutch with simply supported edge

Figures 4 and 5 show the variation of the first two-order dimensionless complex frequencies ω of the rotating circular plate in friction clutch with the dimensionless angular speed for $\psi_1 = 0$, $\psi_2 = 0.1$ and $\psi_3 = 0.3$. When the

Table 1. First four-order dimensionless natural frequencies of the nonrotating plate with different boundary conditions.

Boundary condition	Natural frequency	$N = 9$	$N = 10$	$N = 11$	$N = 13$	$N = 15$	Results in Ni[37]
Simply supported	ω_1	4.943	4.943	4.943	4.943	4.943	4.997
	ω_2	29.782	29.776	29.775	29.774	29.774	29.76
	ω_3	73.126	74.469	74.291	74.294	74.293	74.20
	ω_4	151.833	134.344	139.770	138.611	138.578	–
Clamped	ω_1	10.226	10.226	10.226	10.225	10.225	10.21
	ω_2	39.803	39.810	39.810	39.811	39.811	39.78
	ω_3	89.955	89.134	89.192	89.194	89.194	89.10
	ω_4	170.414	160.884	158.051	158.351	158.352	158.13
Free	ω_1	0	0	0	0	0	0
	ω_2	9.026	9.023	9.024	9.023	9.023	9.084
	ω_3	38.609	38.583	38.523	38.523	38.523	38.55
	ω_4	84.729	88.412	88.289	87.915	87.935	87.80

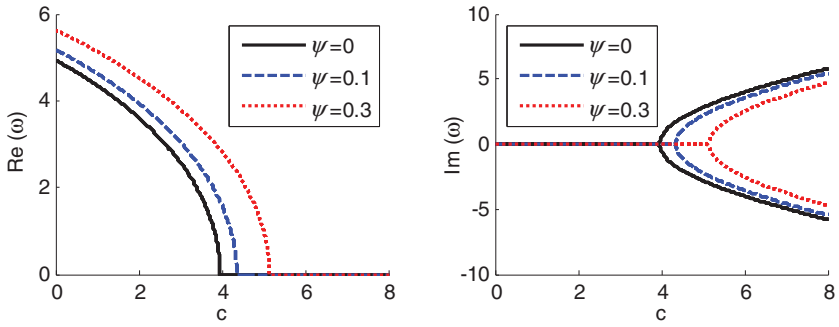

Figure 4. First-order dimensionless complex frequency versus dimensionless angular speed (simply supported edge).

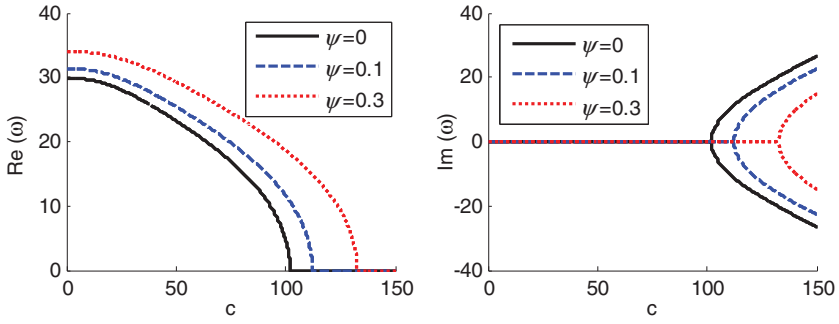

Figure 5. Second-order dimensionless complex frequency versus dimensionless angular speed (simply supported edge).

Table 2. First two-order dimensionless natural frequencies of the rotating circular plate in friction clutch ($c = 0$).

	$\psi_1 = 0$	$\psi_2 = 0.1$	$\psi_3 = 0.3$
ω_1	4.943	5.184	5.642
ω_2	29.774	31.272	33.915

angular speed $c = 0$, the first two-order dimensionless complex frequencies ω_1 and ω_2 are real numbers, as shown in Table 2. The first two-order dimensionless natural frequencies of the nonrotating circular plate in the case of thermoelastic coupling are larger than those in the case of the uncoupling. The reason is that the dimensionless thermoelastic coupling coefficient $\psi > 0$ is equivalent to the increasing of the flexural rigidity of the plate. As the dimensionless angular speed increases, the real parts of ω become smaller, while their imaginary parts are zero. When the dimensionless angular speed reaches a certain critical speed shown in Table 3, the real parts in the first-order and second-order modes become zero, but their imaginary parts have two branches. The result shows that the divergence instability appears in the first-order and second-order modes of the rotating circular plate when the dimensionless angular speed is larger than the critical divergence speed.

Figure 6 indicates the variation of the first-order complex frequency of the rotating circular plate in friction clutch with the dimensionless thermoelastic coupling coefficient ψ for $c = 3.96$ (the critical divergence speed in first-order mode when $\psi = 0$), $c = 2$ and $c = 6$. In the case of $c = 3.96$, the real part increases gradually from zero to positive values as ψ increases, while its imaginary part is zero. This result is consistent with the critical divergence speed in Wang et al.,[5] which proves the correctness of the calculation in this study. In the case of $c = 2 < 3.96$, the increase in ψ leads to the increase of the real part of the first-order complex frequency, while its imaginary part is zero. In the case of $c = 6 > 3.96$ and $\psi < 0.51$, the real part of the first-order complex frequency remains zero with the increase of ψ, while two branches appear in its imaginary part. The rotating circular plate exhibits divergence instability until the two branches of the imaginary part merge with each other at $\psi = 0.51$. In the case of $c = 6 > 3.96$ and $\psi > 0.51$, $\mathrm{Re}(\omega) > 0$ and $\mathrm{Im}(\omega) = 0$ indicate the stability of the rotating

Table 3. Critical divergence speed of the circular plate in the first-order and second-order modes (simply supported edge).

	$\psi_1 = 0$	$\psi_2 = 0.1$	$\psi_3 = 0.3$
c_1	3.96	4.32	5.16
c_2	101.9	112.1	132.5

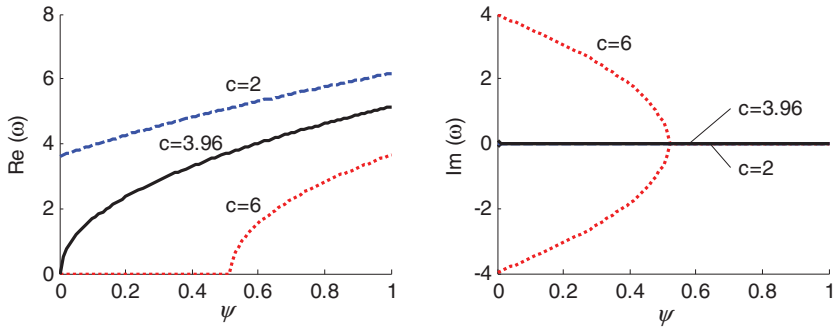

Figure 6. First-order dimensionless complex frequency versus dimensionless thermoelastic coupling coefficient (simply supported edge).

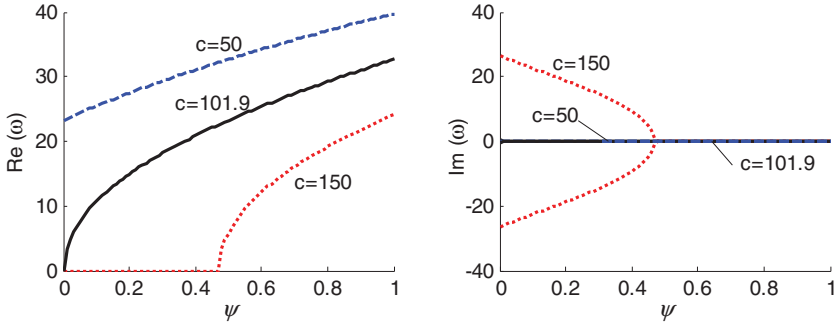

Figure 7. Second-order dimensionless complex frequency versus dimensionless thermoelastic coupling coefficient (simply supported edge).

circular plate in the first-order mode. $\psi = 0.51$ is the critical dimensionless thermoelastic coupling coefficient in the first-order mode for $c = 6$.

Figure 7 presents the variation of the second-order complex frequency of the rotating circular plate in friction clutch with the dimensionless thermoelastic coupling coefficient for $c = 101.9$ (the critical divergence speed in second-order mode when $\psi = 0$), $c = 50$ and $c = 150$. By comparing Figures 7 and 6, we can see that the effect of the angular speed on the second-order complex frequency is similar to that on the first-order complex frequency. In the case of $c = 101.9$ and $c = 50 < 101.9$, the real part remains positive values, while its imaginary part is zero. This result indicates that the rotating circular plate is stable. In the case of $c = 150 > 101.9$, $\psi = 0.47$ is the critical dimensionless thermoelastic coupling coefficient in the second-order mode for $c = 150$ and denotes the critical point from the instability and stability.

Figure 8(a) and (b) shows the effects of the dimensionless thermoelastic coupling coefficient on the first two-order critical divergence speeds. It can be seen in Figure 8 that, with the increase of the dimensionless thermoelastic coupling coefficient, the first two-order critical divergence speeds of the rotating circular plate with simply supported edge increase.

Rotating circular plate in friction clutch with clamped edge

Figures 9 and 10 show the variation of the first two-order dimensionless complex frequencies ω of the rotating circular plate in friction clutch with the dimensionless angular speed for $\psi_1 = 0$, $\psi_2 = 0.1$ and $\psi_3 = 0.3$.

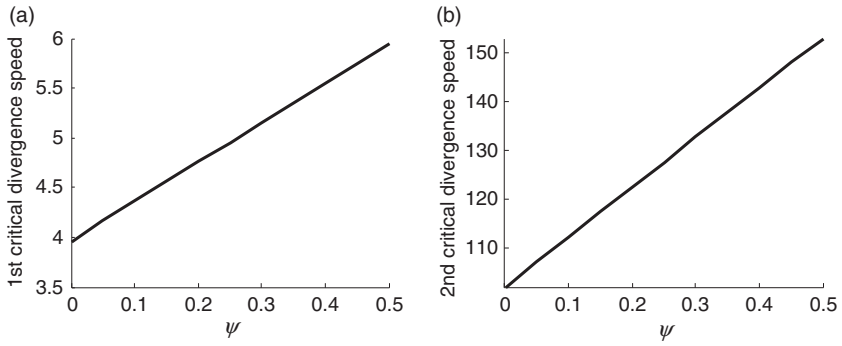

Figure 8. First two-order critical divergence speeds versus dimensionless thermoelastic coupling coefficient: (a) first order and (b) second order.

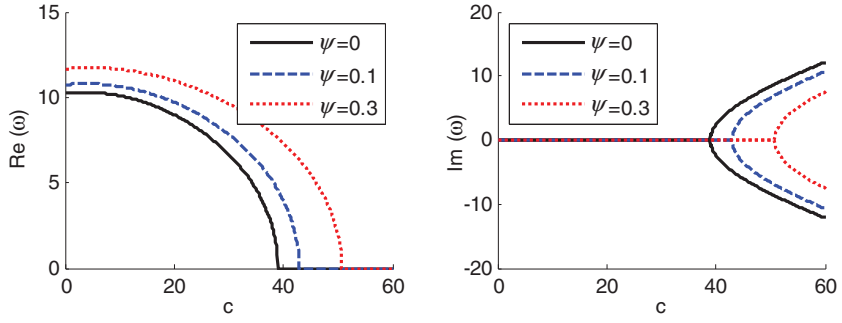

Figure 9. First-order dimensionless complex frequency versus dimensionless angular speed (clamped edge).

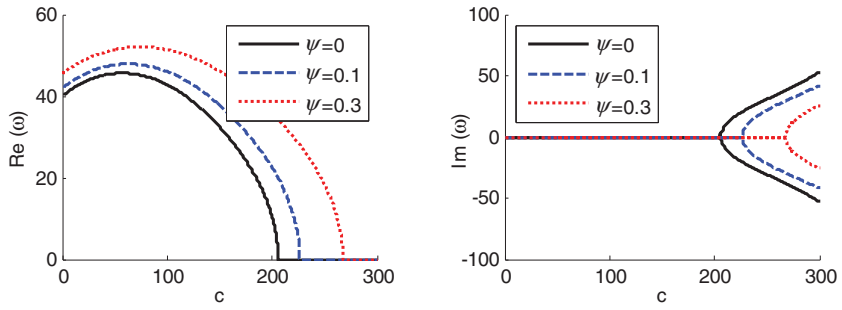

Figure 10. Second-order dimensionless complex frequency versus dimensionless angular speed (clamped edge).

An increase in the dimensionless angular speed causes the real parts of ω to increase firstly and then decrease; subsequently, their imaginary parts become two branches. The result notes that the first two-order modes exhibit the divergence instability. This instability of the rotating circular plate in clutch with clamped edge is similar to that with simply supported edge. Table 4 presents the critical divergence speeds in the first-order and second-order modes.

Figures 11 and 12 indicate the variation of the first two-order dimensionless complex frequencies ω of the rotating plate in clutch with the dimensionless thermoelastic coupling coefficient for a certain angular speed, respectively. By comparing Figures 11 and 12 with Figures 6 and 7, we can see that the change curve of ω with the dimensionless thermoelastic coupling coefficient of the clamped plate is similar to that of the simply supported plate. When the angular speed ($c = 39.1$, $c = 20$, $c = 205.9$ and $c = 100$) is less than or equal to the critical angular speed ($\psi_1 = 0$), the first-order and second-order modes of the rotating circular plate in clutch remain stable. When the angular speed ($c = 100$ and $c = 250$) is larger than the critical angular speed, the first-order and second-order

Table 4. Critical divergence speed of the rotating circular plate in the first-order and second-order modes (clamped edge).

	$\psi_1 = 0$	$\psi_2 = 0.1$	$\psi_3 = 0.3$
c_1	39.1	43.0	50.8
c_2	205.9	226.5	267.5

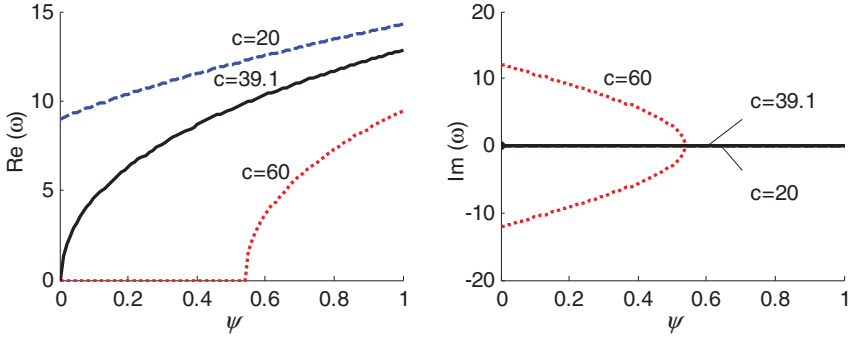

Figure 11. First-order dimensionless complex frequency versus dimensionless thermoelastic coupling coefficient (clamped edge).

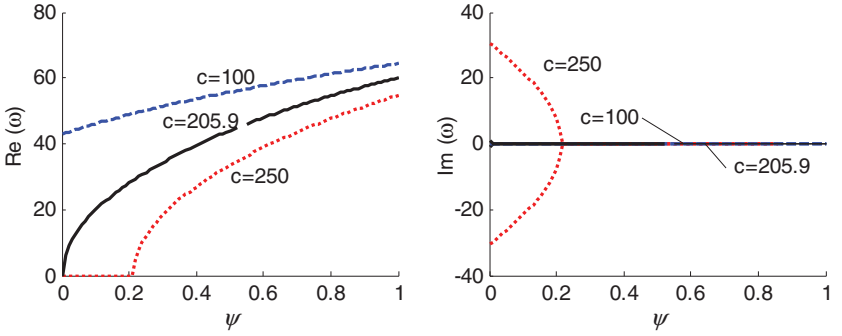

Figure 12. Second-order dimensionless complex frequency versus dimensionless thermoelastic coupling coefficient (clamped edge).

modes change from divergence instability to stability with the increase of the dimensionless thermoelastic coupling coefficient. The critical dimensionless thermoelastic coupling coefficients existing in the first-order and second-order modes are not only dependent on the boundary condition but also affected by the angular speed.

Figure 13(a) and (b) shows the variation of the first two-order critical divergence speed with the dimensionless thermoelastic coupling coefficient. With the increase of the dimensionless thermoelastic coupling coefficient, the first two-order critical divergence speeds of the rotating circular plate with clamped edge increase.

Rotating circular plate in friction clutch with free edge

Figures 14 and 15 show the variation of the first two-order dimensionless complex frequencies ω of the rotating circular plate in friction clutch with the dimensionless angular speed for $\psi_1 = 0$, $\psi_2 = 0.1$ and $\psi_3 = 0.3$. As shown in Figures 14 and 15, the real parts of the first two-order complex frequencies of the rotating circular plate increase with the increase of the dimensionless angular speed. In addition, the real parts increase with the increase of the dimensionless thermoelastic coupling coefficient for the same angular speed, while their imaginary parts are zero. Therefore, the critical divergence speed and critical dimensionless thermoelastic coupling coefficient do not exist, and the instability does not occur. The reason is that the normal in-plane forces N_r and N_θ for a completely free plate subject to a linearly distributed radial inertial force are tensile stresses. With the increase of the angular speed, N_r and N_θ increase linearly, and the deflection of circular plate decease; thus the real parts increase.

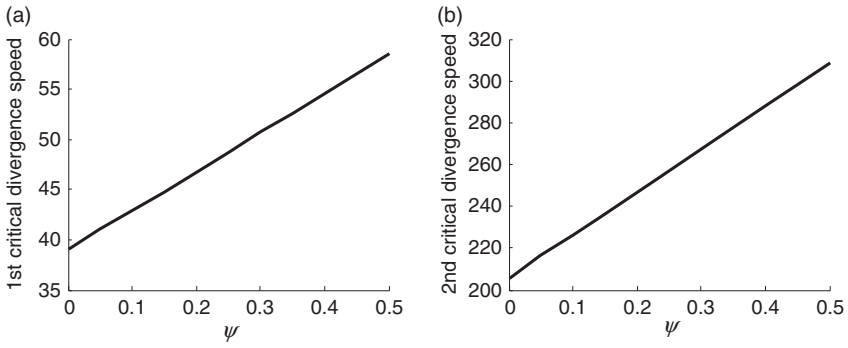

Figure 13. First two-order critical divergence speeds versus dimensionless thermoelastic coupling coefficient: (a) first order and (b) second order.

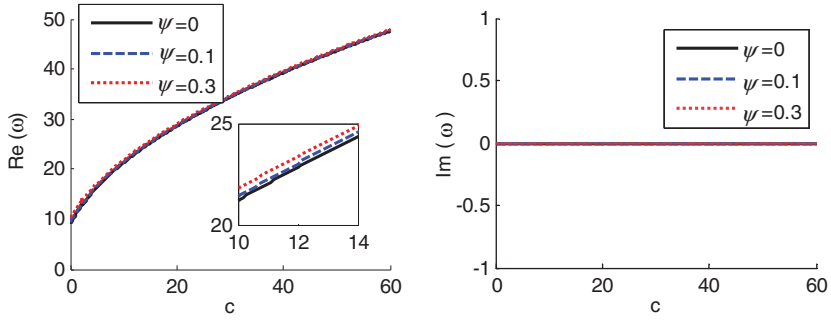

Figure 14. First-order dimensionless complex frequency versus dimensionless angular speed (free edge).

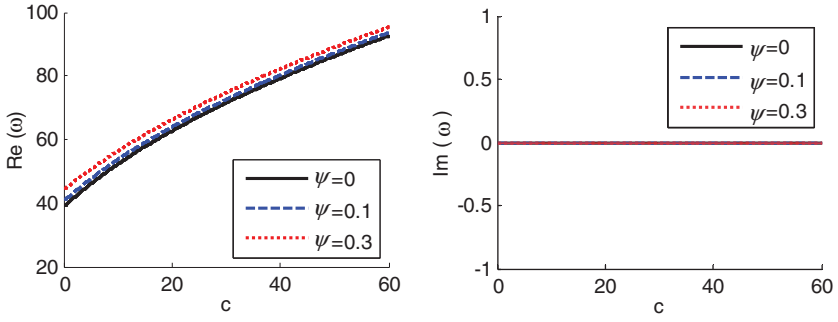

Figure 15. Second-order dimensionless complex frequency versus dimensionless angular speed (free edge).

Conclusions

The rotating circular plate in friction clutch of the Shaanxi XUST-18 explosion-proof mineral locomotive is selected to examine. The thermoelastic coupling transverse vibration and stability of the rotating circular plate in friction clutch with three boundaries are investigated by DQM. The effects of the dimensionless angular speed, the dimensionless thermoelastic coupling coefficient and the boundary condition on transverse vibration and stability are discussed. The results are listed as follows:

1. As the dimensionless angular speed increases, the real parts of the first two-order dimensionless complex frequencies decrease to zero under the boundary condition of simple supported edge. However, the real parts increase firstly and then decrease to zero under the boundary condition of clamped edge and increase in the range of positive values under the boundary condition of free edge.
2. The first two-order modes exhibit divergence instability under the boundary conditions of simple supported and clamped edges, and the corresponding critical divergence speed in the case of thermoelastic coupling is larger than that in the case of uncoupling. With the increase of the dimensionless thermoelastic coupling

coefficient, the critical divergence speed increases under the boundary conditions of simple supported and clamped edges. However, the instability does not occur under the boundary condition of free edge, and the critical divergence speed does not exist.

3. When the dimensionless angular speed is larger than the critical divergence speed ($\psi = 0$), the critical dimensionless thermoelastic coupling coefficient exists under the simple supported and clamped edge boundary conditions. The critical dimensionless thermoelastic coupling coefficient is affected not only by the boundary conditions but also by the angular speed.

From these results, this study provides a theoretical basis for optimizing the structure of the friction circular plate in clutch and improving working condition stability for friction clutch.

Declaration of conflicting interests

The author(s) declared no potential conflicts of interest with respect to the research, authorship, and/or publication of this article.

Funding

The author(s) disclosed receipt of the following financial support for the research, authorship, and/ or publication of this article: The authors gratefully acknowledge the support of the National Natural Science Foundation of China (No. 11472211) and the Natural Science Foundation of Education Department of Shaanxi Province of China (No. 2013JK1042).

ORCID iD

Yongqiang Yang http://orcid.org/0000-0002-1625-7148

References

1. Khorasany RMH and Hutton SG. An analytical study on the effect of rigid body translational degree of freedom on the vibration characteristics of elastically constrained rotating disks. *Int J Mech Sci* 2010; 52: 1186–1192.
2. Shojaeefard MH, Googarchin HS, Mahinzare M, et al. Free vibration and critical angular velocity of a rotating variable thickness two-directional FG circular microplate. *Microsyst Technol* 2017; 2017: 1–19.
3. Maretic R. Transverse vibration and stability of an eccentric rotating circular plate. *J Sound Vib* 2005; 280: 467–478.
4. Wang ZM, Gao JB and Li HX. Axially symmetric vibration and stability of circular thin plate subjected to non-conservative forces. *Chin J Solid Mech* 2003; 24: 155–161. (in Chinese)
5. Wang ZM, Wang Z and Zhang R. Transverse vibration analysis of spinning circular plate based on differential quadrature method. *J Vib Shock* 2014; 33: 125–129. (in Chinese)
6. Gupta AK, Agarwala N and Kaurb H. Transverse vibration of nonhomogeneous orthotropic viscoelastic circular plate of varying parabolic thickness field. *Math Meth Appl Sci* 2011; 34: 2065–2076.
7. Heo JW and Chung JT. Vibration analysis of a flexible rotating disk with angular misalignment. *J Sound Vib* 2004; 274: 821–841.
8. Bauer HF and Eidel W. Transverse vibration and stability of spinning circular plates of constant thickness and different boundary conditions. *J Sound Vib* 2007; 300: 877–895.
9. Hochlenert D, Spelsberg-Korspeter G and Hagedorn P. Friction induced vibrations in moving continua and their application to brake squeal. *J Appl Mech* 2007; 74: 542–549.
10. Mottershead JE and Chan SN. Flutter instability of circular discs with frictional follower loads. *J Vib Acoust* 1995; 117: 161–163.
11. Hu YD and Wang T. Nonlinear resonance of a conductive rotating circular plate in the magnetic field. *J Vib Shock* 2016; 35: 177–181. (in Chinese)
12. Li Z, Hu YD and Li J. Magnetoelastic principal parametric resonance of a rotating electroconductive circular plate. *Shock Vib* 2017; 2017: 1–12.
13. Sepahi O, Forouzan MR and Malekzadeh P. Large deflection analysis of thermo-mechanical loaded annular FGM plates on nonlinear elastic foundation via DQM. *Compos Struct* 2010; 92: 2369–2378.
14. Shu XF and Zhang XQ. The study of nonlinear thermoelastic free vibration of simply supported circular plate. *Eng Mech* 2000; 17: 97–101. (in Chinese)
15. Trajkovski D and Cukic R. A coupled problem of thermoelastic vibrations of a circular plate with exact boundary conditions. *Mech Res Commun* 1999; 26: 217–224.
16. Sun YX and Masumi S. Vibrations of microscale circular plates induced by ultra-fast lasers. *Int J Mech Sci* 2008; 50: 1365–1371.

17. Sun YX and Tohmyoh H. Thermoelastic damping of the axisymmetric vibration of circular plate resonators. *J Sound Vib* 2009; 319: 392–405.
18. Salajeghe S, Khadem SE and Rasekh M. Nonlinear analysis of thermoelastic damping in axisymmetric vibration of micro circular thin-plate resonators. *Appl Math Model* 2012; 36: 5991–6000.
19. Hao ZL. Thermoelastic damping in the contour-mode vibrations of micro- and nano-electromechanical circular thin-plate resonators. *J Sound Vib* 2008; 313: 77–96.
20. Kumar R, Kaushal P and Sharma R. Axisymmetric vibration for micropolar porous thermoelastic circular plate. *Int J Appl Mech Eng* 2017; 22: 583–600.
21. Bhada P, Vargheseb V and Khalsac L. Thermoelastic-induced vibrations on an elliptical disk with internal heat sources. *J Therm Stresses* 2016; 40: 502–516.
22. Wang Y, Tian Z and Wu JM. Dynamic stability of an axially moving paper board with added subsystems. *J Low Frequency Noise Vib Active Control* 2018; 37: 48–59.
23. Yayli MO. Free vibration analysis of a single-walled carbon nanotube embedded in an elastic matrix under rotational restraints. *Micro Nano Lett* 2018; 13: 202–206.
24. Yayli MO. Free longitudinal vibration of a nanorod with elastic spring boundary conditions made of functionally graded material. *Micro Nano Lett* 2018; 13: 1031–1035.
25. Yayli MO. A compact analytical method for vibration analysis of single-walled carbon nanotubes with restrained boundary conditions. *J Vib Control* 2016; 22: 2542–2555.
26. Yayli MO. Buckling analysis of a microbeam embedded in an elastic medium with deformable boundary conditions. *Micro Nano Lett* 2016; 11: 741–745.
27. Yayli MO. Buckling analysis of Euler columns embedded in an elastic medium with general elastic boundary conditions. *Mech Based Des Struc* 2017; 46: 110–122.
28. Wu JM, Shao MY, Wang Y, et al. Stability analysis of moving printing web with sine half-wave variable density based on differential quadrature method. *J Vib Acoust* 2017; 139: 061018.
29. Bert CW and Malik M. Differential quadrature: a powerful new technique for analysis of composite structures. *Compos Struct* 1997; 39: 179–189.
30. Alibeigloo A and Emtehani A. Static and free vibration analyses of carbon nanotube reinforced composite plate using differential quadrature method. *Meccanica* 2015; 50: 61–76.
31. Han JB and Liew KM. Analysis of moderately thick circular plates using differential quadrature method. *J Eng Mech-ASCE* 1997; 123: 1247–1252.
32. Shu C and Chen W. On optimal selection of interior points for applying discretized boundary conditions in DQ vibration of beams and plates. *J Sound Vib*. 1999; 222: 239–257.
33. Wang HG. *Introduction to thermoelasticity*. Beijing: Tsinghua University Press, 1989. (in Chinese)
34. Guo XX and Wang ZM. Analysis of the coupled thermoelastic vibration for axially moving beam. *J Sound Vib*. 2009; 325: 597–608.
35. Wang Y, Cao X and Jing T. Dynamic characteristics and stability of axially moving viscoelastic plate with piezoelectric layer. *J Low Frequen Noise Vib Active Control*. 2014; 33: 341–356.
36. Wu JM, Wu QM and Ma LE. Parameter Vibration and Dynamic Stability of the Printing Paper Web with Variable Speed. *J Low Frequen Noise Vib Active Control*. 2010; 29: 281–291.
37. Ni ZH. *Vibration mechanics*. Xi'an: Xi'an Jiaotong University Press, 1994. (in Chinese)